

Characterization of shear rates in airlift bioreactors for animal cell culture

Emilio Molina Grima^a, Yusuf Chisti^{b,*}, Murray Moo-Young^b

^a *Departamento de Ingeniería Química, Universidad de Almería, E-04071 Almería, Spain*

^b *Department of Chemical Engineering, University of Waterloo, Waterloo, Ont. N2L 3G1, Canada*

Received 15 August 1996; received in revised form 18 February 1997; accepted 28 February 1997

Abstract

A well established analysis of energy dissipation in the riser, downcomer and the bottom sections of split-cylinder airlift bioreactors (aspect ratio = 7.6 and 14.5; equal riser-to-downcomer cross-sectional area ratios of 1.0) was used to characterize shear rates in those systems for application to animal cell culture. Shear rates were evaluated for suspensions of typical microcarriers (loading = 0–30 kg m⁻³; particle diameter = (150–300) × 10⁻⁶ m; density 1030–1050 kg m⁻³) encountered in anchorage-dependent cell culture and for microcarrier-free liquids. For the reactors tested, the highest shear rates were encountered in the bottom zone; the riser had lower shear rate values, while the downcomer was the most quiescent. The shear rates in various zones ranged over 0–12 000 s⁻¹ for a riser superficial gas velocity range of 0–6.7 × 10⁻³ m s⁻¹ which is typical for cell culture. In all zones, the shear rates increased with increasing aeration rate. Shear rates declined with increasing loading of microcarriers, but were not substantially affected by the carrier diameter or density. Relative to the microcarrier free system, even small amounts of carriers (6 kg m⁻³) lowered the maximum prevailing shear rate to about 4000 s⁻¹. The shear rates were extremely sensitive to the length scale of the fluid eddies when the eddy length-to-carrier diameter ratio was less than or equal to unity. The results showed quantitatively how the shear rate in various zones of airlift reactors may be manipulated by modifications to operational and geometric parameters. The methodology presented allowed for characterization of shear rates in the bulk flow, unlike existing studies that provide information only on wall shear rates which are not particularly relevant to shear sensitive bioprocesses. © 1997 Elsevier Science B.V.

Keywords: Airlift bioreactor; Shear stress; Shear rate; Animal cell culture

1. Introduction

Animal cell culture is the mainstay of producing therapeutic, diagnostic and protective proteins that have wide ranging commercial and social significance. Two types of culture methods domi-

* Corresponding author. Tel.: +1 519 8884567, ext. 5254; fax: +1 519 7464979.

nate in industrial practice: free suspension culture in which cells are freely suspended in a nutrient broth; and microcarrier culture in which anchorage dependent cells grow on surfaces of solid carriers that are suspended in a culture fluid. Irrespective of the culture method, the suspending fluid is invariably directly sparged with air or other gas mixture to supply the cells with oxygen. Stirred tank bioreactors are the predominant type of culture vessels, although some of the largest reactors for free suspension culture are known to be draft tube internal-loop airlift devices (Birch et al., 1987). Airlift bioreactors are particularly robust with respect to long-term sterile operation and they have other advantages (Chisti, 1989). However, a lack of information on hydrodynamic shear forces in airlift devices poses design and scale-up uncertainties for shear sensitive animal cells. Here we review relevant data on susceptibility of animal cells to hydrodynamic forces and develop methods for estimation of these forces in different zones of airlift bioreactors.

2. Literature

Airlift bioreactors may be applied to culture of freely suspended animal cells (Arathoon and Birch, 1986; Birch et al., 1987) or to cells anchored on microcarriers (Ganzeveld et al., 1995). In both cases, the cells would be subject to aeration and fluid turbulence. Consequently, mechanical forces associated with bubbling phenomena, and fluid shear with respect to cells on solid surfaces as well as cells in suspension need to be considered.

In studies with rat aortic endothelial cells anchored on internal walls of glass capillaries, laminar shear stress was shown to affect the cytosolic pH because of preferential leakage of certain ions out of the cells into the saline buffer (Ziegelstein et al., 1992). This permeability enhancement occurred even at stress levels as low as 0.05 N m^{-2} applied over short durations (~ 2 min). While low levels of shear stress may have physiologically significant effects, higher levels are needed for physical damage. Numerical analysis of the forces exerted by laminar flow on anchorage dependent

cells attached to flat surfaces suggests that a shear stress between 0.25 and 0.6 N m^{-2} is sufficient to detach round cells, but much higher values are needed to dislodge spread out cells (Olivier and Truskey, 1993). These observations are relevant to microcarrier culture where, during inoculation, the round cells must first attach to microcarriers before spreading on the solid surface. During proliferation, bead-to-bead transfer of cells may also require a level of turbulence that is not so high as to hinder the reattachment process, yet not so low that bead-to-cell encounters are few.

In microcarrier culture, collisions between microcarriers and interactions between carriers and the internals of a reactor are other possible causes of cell damage, particularly in stirred bioreactors (Cherry and Papoutsakis, 1988, 1989; Papoutsakis, 1991). However, in airlift bioreactors with typical microcarriers and the usual low rates of power input, bead-to-bead collisions are rare, as visually observed by Ganzeveld et al. (1995): microcarriers move along parallel paths, following the laminar fluid streamlines, without interacting with themselves or with the internals of the bioreactor. In highly agitated or aerated systems, the length scale of fluid eddies can be of the same order as the dimensions of microcarriers, resulting in higher relative velocities between the solid and the liquid phases and possible damage to cells (Cherry and Papoutsakis, 1986; Papoutsakis, 1991; Chisti, 1993).

The shear sensitivity of freely suspended hybridomas in a laminar shear stress Couette flow device has been tested while the fluidity of the plasma membrane was manipulated by additives and by temperature changes (Ramírez and Mutharasan, 1990). Conditions that yielded higher membrane fluidity produced more fragile cells (Ramírez and Mutharasan, 1990). Experiments with Pluronic F68, a non-ionic surfactant, showed that the surfactant decreased the membrane fluidity, suggesting that the well known protective effect of Pluronic F68 was linked with its interactions with the plasma membrane. Similarly, the often reported shear protective effect of serum has been hypothesized to originate at least partly from its ability to reduce membrane fluidity (Ramírez and Mutharasan, 1990, 1992). Choles-

terol enrichment of the culture medium also reduced membrane fluidity and enhanced the shear resistance of hybridomas (Ramírez and Mutharasan, 1992). Other data suggest that the protective effect of Pluronic F68 may not be quite general (Zhang et al., 1995). For porcine erythrocytes suspended in isotonic buffer, Zhang et al. (1995) noted that addition of Pluronic F68 actually increased cell lysis in agitated environments relative to results in the surfactant free medium. Other media additives that have been examined for potential effects on cell survival include albumin (Zhang et al., 1995), dextran (Chattopadhyay et al., 1995a; Michaels et al., 1992; Zhang et al., 1995), polyvinyl alcohol (Chattopadhyay et al., 1995a; Michaels and Papoutsakis, 1991; Michaels et al., 1992, 1995a,b), polyethylene glycol (Chattopadhyay et al., 1995a; Michaels and Papoutsakis, 1991; Michaels et al., 1995a,b), methyl cellulose (Chattopadhyay et al., 1995a; Michaels et al., 1992, 1995a,b), and polyvinyl pyrrolidone (Michaels et al., 1995a,b). Most of these additives are viscosity enhancers that are not widely used in commercial culture.

Using flow cytometry, Al-Rubeai et al. (1993) showed that leakage of a positively charged dye, fluorescein diacetate, from murine hybridomas increased with rising intensity of agitation, thus suggesting a possible link between permeability of cell membrane and shear rate. However, because intense agitation was accompanied by entrainment of gas bubbles into the culture (Al-Rubeai et al., 1993), the observed leakage could not be conclusively associated with fluid turbulence. The authors noted that for otherwise fixed agitation conditions, the leakage of the dye reduced when the culture medium was formulated with 1% Pluronic-F68. For the hybridoma line of Al-Rubeai et al. (1993), Born et al. (1992) reported that exposure to shear stress (208 N m^{-2}) in laminar flow in a cone and plate viscometer (no aeration) led to substantial loss in cell count and viability within 20 min. At a constant 180 s exposure, increasing shear stress over $100\text{--}350 \text{ N m}^{-2}$ linearly enhanced cell disruption, with $>90\%$ of the cells being destroyed at 350 N m^{-2} stress level (Born et al., 1992).

Damage to murine hybridomas was observed by Jan et al. (1993) in stirred tanks equipped with marine impellers agitated at sufficiently high speeds that vortexing occurred and gas entrained into the medium. Even at these high speeds damage could be prevented by baffling the tank which suppressed vortex formation. Usually though, vortexing is not a problem in large scale cell culture. Unbaffled, marine impeller stirred tanks were successfully used by Chisti (1993) in industrial culture of several hybridoma lines. The effects of agitation on hybridoma culture in the absence of sparging or surface entrainment were further examined by Smith and Greenfield (1992). Culture growth was unaffected by agitation intensity (100 or 600 rpm) in the RPMI medium supplemented with fetal bovine serum (10% v/v). However, in PFHM II medium supplemented with either Pluronic F68, fetal bovine serum, or bovine serum albumin, and agitated at 600 rpm (impeller tip speed = 1.6 m s^{-1} , power input = 1 kW m^{-3}) the results were different: the agitation intensity did not affect the exponential growth rate, but once growth had ceased, the decline phase was substantially faster than in control experiments (Smith and Greenfield, 1992).

Clearly, fluid mechanical forces other than those associated with aeration do affect cells. Even highly robust cells are known to be affected by intense shear fields: disruption of microbial cells by high pressure homogenization is well known (Chisti and Moo-Young, 1986). Shear sensitivity of plant cells has been reviewed by Doran (1993).

Cell lines differ tremendously in sensitivity to aeration as was demonstrated by Handa et al. (1987). At constant aeration rates in geometrically identical bubble columns, smaller diameter bubbles (0.2 mm diameter) were shown to be significantly more damaging to a hybridoma than larger bubbles (1.62 mm diameter). In industrial scale cultures of several hybridomas, Chisti (1993) preferred yet larger bubbles (10–20 mm diameter) for aeration. However, the effect of bubble size may not be prevalent across cell types. Thus, in another study, baby hamster kidney (BHK-21) cells were not sensitive to the size of gas bubbles (Handa-Corrigan et al., 1989). Over a superficial

gas velocity range of $(0.42\text{--}8.5) \times 10^{-4} \text{ m s}^{-1}$, higher velocities led to faster decline in cell viability of a hybridoma (Handa et al., 1987) which is consistent with other similar observations (Martens et al., 1992). The presence of Pluronic F68 (0.1% v/v) in the medium suppressed cell damage over the entire range of aeration rates (Handa et al., 1987). The protective effect of the surfactant increased with its concentration, but levelled off at $\sim 0.15\%$ v/v. Quite apart from influencing the fluidity of plasma membrane, Pluronic F68 is known to reduce the attachment of cells to bubbles (Garcia-Briones and Chalmers, 1992; Handa-Corrigan et al., 1989; Trinh et al., 1994). Rupture of 3.5 mm single bubbles in suspensions of *Spodoptera frugiperda* SF9 insect cells was observed to kill cells; the kill was reduced in Pluronic F68 supplemented suspensions apparently because fewer cells attached to bubbles (Trinh et al., 1994).

Aeration of suspended cells with excessively small bubbles has been associated with cell 'wash out' into a stable foam layer by a froth flotation mechanism in large scale bioreactors (Chisti, 1993; Chisti and Moo-Young, 1996). Other similar observations have been reported (Michaels et al., 1995a). Microscopic visualization studies have confirmed cell attachment to bubbles (Bavarian et al., 1991; Chalmers and Bavarian, 1991), and a thermodynamic explanation of cell adhesion has been propounded (Chattopadhyay et al., 1995b). Larger bubbles with higher rise velocities have been found effective in reducing cell attachment and wash out (Chisti, 1993). In addition, larger bubbles produce less stable foams. As noted earlier, such bubbles have been favoured in aeration.

In suspension culture of several types of animal cells in small bubble columns (diameter = 0.05 m; $h_L = 0.05\text{--}1.0 \text{ m}$) fetal calf serum had a shear protective effect which depended on the concentration of serum (Handa-Corrigan et al., 1989). The greatest level of protection occurred at 10% FCS for BHK-21 cells (Handa-Corrigan et al., 1989). At constant aeration rate ($5 \text{ cm}^3 \text{ min}^{-1}$), the survival of myeloma and hybridoma lines was enhanced as the height of liquid in the column increased (Handa-Corrigan et al., 1989). This result was qualitatively consistent with other reports

(Tramper et al., 1987; Martens et al., 1992; van der Pol et al., 1992) supporting the view that cell death occurred predominantly in the bubble disengagement zone at the surface (Handa et al., 1987; Handa-Corrigan et al., 1989). Data cited by Doran (1993) suggest that shear stress levels associated with bubble rupture at the surface may range over $100\text{--}300 \text{ N m}^{-2}$. These values are remarkably consistent with shear rates that damaged hybridomas in the unaerated laminar flow experiments of Born et al. (1992).

Based on the energetics of bubble associated damage to freely suspended cells, Wang et al. (1994) concluded that the principal determinants of cell damage were cell-bubble encounter rate, the rate of bubble breakup within the fluid and the bursting rate at the surface. Cell death correlated linearly with specific gas-liquid interfacial area, with the proportionality constant being 0.0125 m h^{-1} for a murine hybridoma (Wang et al., 1994). Computer simulations of bubble rupture at gas-liquid surface suggest high rates of localized energy dissipation that may damage cells in the vicinity (Garcia-Briones and Chalmers, 1994; Garcia-Briones et al., 1994). The rate of energy dissipation depends inversely on the size of the collapsing bubble (Boulton-Stone and Blake, 1993; Garcia-Briones and Chalmers, 1994)—an observation that is consistent with the earlier empirically established preference for larger bubbles in aeration (Chisti, 1993).

In keeping with widely noted findings (Handa-Corrigan et al., 1989; Martens et al., 1992), van der Pol et al. (1992) observed that reduction in fetal calf serum level from 2.5 to 0% substantially increased the death rate constant of a hybridoma in aerated culture. Investigations revealed that serum had no long-term biological effect, but only a direct non-specific physical protective effect (van der Pol et al., 1992). The first order death rate constant (k_d) in a bubble column followed the equation (van der Pol et al., 1992)

$$k_d = \frac{4QV_k}{\pi d_c^2 h_L} \quad (1)$$

that was originally introduced for insect cells by Tramper et al. (1987). In Eq. (1), Q is the volumetric aeration rate, h_L is the height of fluid, d_c is

the column diameter and V_k is a hypothetical dimensionless specific killing volume (Tramper et al., 1987). Eq. (1) has applied also to airlift reactors where the protective effect of serum has been claimed to have physiological origins (Martens et al., 1992). Note that increasing the liquid level at constant aeration rate in a column of fixed diameter decreases the specific power input.

The studies reviewed here conclusively demonstrate that animal cells are affected, but not necessarily disrupted, even by low levels of hydrodynamic shear rates quite independently of any gas bubble associated effects. Aeration clearly affects cells, but control of bubble size, aeration rate and the use of additives mitigate this effect. While the effects of shear rate per se on cells are increasingly better understood in such defined geometries as capillaries and viscometers, quantification of shear rates in complex hydrodynamic environments of bioreactors remains elusive. Even in relatively simple devices such as bubble columns, the several available correlations for average shear rate produce dramatically different values (Chisti and Moo-Young, 1989; Shi et al., 1990). Moreover, those correlations have other mechanistic flaws (Chisti and Moo-Young, 1989; Chisti, 1989). For airlift reactors that are of particular interest in large scale animal cell culture (Arathoon and Birch, 1986; Birch et al., 1987), shear rate data is even more limited.

For an external loop airlift reactor, an empirically determined equation for 'effective' shear rate is due to Shi et al. (1990):

$$\gamma = 3.26 - 3.51 \times 10^2 U_{Gr} + 1.48 \times 10^4 U_{Gr}^2 \quad (2)$$

Eq. (2) was developed for $0.004 < U_{Gr} < 0.06$ m s⁻¹; the shear rate range covered was 2–35 s⁻¹. The methodology used in obtaining Eq. (2) implied that the shear rate values were strictly wall shear rates, not the bulk fluid mean shear rates as suggested by Shi et al. (1990). The external-loop configuration in which the equation was developed is almost never used for cell culture or other industrial fermentations. Further, the shear rate values generated by Eq. (2) do not agree with values that may be calculated from well known principles of fluid mechanics. Thus, the wall shear stress in a flow channel such as the riser or the

downcomer of an airlift reactor may be estimated with the mechanistic relationship

$$\tau_w = \frac{1}{2} C_f \rho_L V_{Lr}^2 \quad (3)$$

and the corresponding shear rate may be calculated as $\gamma_w = \tau_w / \mu_L$. The Fanning friction factor C_f may be calculated with Eq. (12) given in the next section. From these equations, the shear stress can be shown to depend on the viscosity of the fluid: $\tau_w \propto \mu_L^{-0.75}$. Eq. (2) does not show any such dependence even though fluids having different viscosities were used in establishing it. Fig. 1 compares the shear rate calculated using Eq. (2) with that obtained from Eq. (3). The disparity between the two procedures is obvious. Of particular significance is the fact that Eq. (2) substantially underpredicts the shear rate at low gas velocities that are relevant to animal cell culture. Note that the comparison in Fig. 1 is for an air-water system and the liquid velocity values used in the computations were calculated with the equation

$$V_{Lr} = 1.55 \left(\frac{A_d}{A_r} \right)^{0.74} U_{Gr}^{1/3} \quad (4)$$

Eq. (4) was established by Bello (1981) for external-loop airlift vessels that were geometrically close to the reactor used by Shi et al. (1990) in

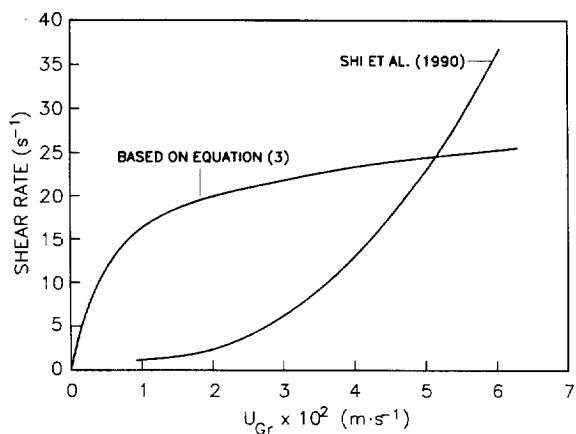


Fig. 1. Calculated wall shear rates in air-water system in an external-loop airlift reactor ($d_r = 0.194$ m; $A_d/A_r = 0.11$; $h_L \approx 1.4$ m) as a function of superficial gas velocity in the riser: Comparison of Eq. (2) of Shi et al. (1990) with shear rate derived from Eq. (3) and Eq. (30).

developing Eq. (2). In view of the uncertainties, there remains a strong need for methods, particularly mechanistic methods, for calculation of shear rates in airlift bioreactors. Because the fluid turbulence intensities in different zones—the riser, the downcomer, the bottom and the top—of such reactors are different (Chisti, 1989), the need is for methods that allow calculation of mean shear rate levels in individual zones rather than a single overall value. This point is important because high shear rates may be confined to particular cell damaging zones, yet the overall level of shear may be deceptively low. In micro-carrier culture, the shear stress at the solid-liquid interface also needs to be known. This paper presents an energy dissipation approach to calculation of shear rates in airlift bioreactors. Relative magnitudes of shear forces in different zones of the reactor are discussed. The calculations are based on experimental hydrodynamic measurements such as gas holdup, aeration rate and the liquid circulation velocity.

3. Theory

The intensity of turbulence and, hence, the shear rates or velocity gradients in a fluid are dependent on the rate of energy dissipation. The latter is different in different zones of an airlift reactor as noted by Chisti et al. (1988). That energy dissipation analysis (Chisti et al., 1988; Chisti, 1989) was used to characterize the shear rates in the riser, the downcomer and the bottom sections of split-cylinder internal-loop airlift reactors as employed by Ganzeveld et al. (1995). Evaluation of the energy input and dissipation rates is discussed below.

3.1. Energy dissipation rate

The rate of energy input into the reactor was determined with the equation

$$E_{in} = QP_a \ln \left(1 + \frac{\rho_L(1 - \varepsilon_G)gh_D}{P_a} \right), \quad (5)$$

where P_a is the atmospheric pressure. Eq. (5) applies for isothermal expansion of the aeration

gas as it moves from the bottom to the top of the reactor. The height of gas-liquid dispersion (h_D) in Eq. (5) was calculated from the known liquid level (h_L) and the overall gas holdup; thus

$$h_D = \frac{h_L}{1 - \varepsilon_G}. \quad (6)$$

For internal-loop airlift reactors such as the split-cylinder vessels used by Ganzeveld et al. (1995), Chisti (1989) noted that the overall gas holdup, ε_G , is related to the holdups in the riser and the downcomer; thus,

$$\varepsilon_G = \frac{A_r \varepsilon_{Gr} + A_d \varepsilon_{Gd}}{A_r + A_d}. \quad (7)$$

Eq. (7) is an analytical relationship that is based on the conservation principle and geometric reasoning (Chisti, 1989). For the reactors used by Ganzeveld et al. (1995), the relationship between the gas holdup in the riser and that in the downcomer was reported to be

$$\varepsilon_{Gd} = 0.63\varepsilon_{Gr} - 0.0008, \quad (8)$$

Further, the cross-sectional areas of the riser and the downcomer were equal, i.e., $A_r = A_d$ (Ganzeveld et al., 1995); hence, Eq. (7) and Eq. (8) could be combined to yield the following expression for gas holdup in the riser:

$$\varepsilon_{Gr} = \frac{2\varepsilon_G + 0.0008}{1.63}, \quad (9)$$

Thus, the overall gas holdup data of Ganzeveld et al. (1995) could be used to calculate the individual holdups in the riser (Eq. (9)) and the downcomer (Eq. (8)). The calculated values were used to obtain a mean gas holdup in the bottom zone:

$$\varepsilon_{Gb} = \frac{1}{2}(\varepsilon_{Gr} + \varepsilon_{Gd}). \quad (10)$$

The energy loss due to skin friction in the riser was calculated with the equation (Chisti, 1989)

$$E_F = 2C_f U_{Lr}(U_{Lr} + U_{Gr}) \frac{h_D}{d_r} (U_{Lr} A_r). \quad (11)$$

The friction factor (C_f) was determined using Blasius equation:

$$C_f = 0.0792 \left(\frac{\rho_L U_{Lr} d_r}{(1 - \varepsilon_{Gr} - \varepsilon_{Sr}) \mu_L} \right)^{-0.25}, \quad (12)$$

where the hydraulic diameter d_r was 3.35×10^{-2} m. The U_{Lr} in Eq. (12) was calculated from the known phase holdups and the measured linear velocity (V_{Lr}) reported by Ganzeveld et al. (1995):

$$U_{Lr} = V_{Lr}(1 - \varepsilon_{Gr} - \varepsilon_{Sr}). \quad (13)$$

Vand's equation was used to calculate the viscosity of the animal cell microcarrier suspensions employed by Ganzeveld et al. (1995); thus

$$\mu_L = \mu_{Lw}(1 + 2.5\phi_S + 7.25\phi_S^2). \quad (14)$$

In Eq. (14), ϕ_S is the solids holdup in a gas-free slurry. The ϕ_S -values were calculated from the known solids loading (W):

$$\phi_S = \frac{W}{\rho_S}. \quad (15)$$

The holdups of microcarrier beads in the riser, the downcomer and the bottom zones were calculated with the equations

$$\varepsilon_{Sr} = \phi_S(1 - \varepsilon_{Gr}), \quad (16)$$

$$\varepsilon_{Sd} = \phi_S(1 - \varepsilon_{Gd}), \quad (17)$$

and

$$\varepsilon_{Sb} = \frac{1}{2}(\varepsilon_{Sr} + \varepsilon_{Sd}). \quad (18)$$

The energy dissipation rate for turnaround flow of liquid under the baffle at the bottom of the reactor was estimated as specified by Chisti (1989); thus,

$$E_B = \frac{1}{2}\rho_L[V_{Ld}^3 K_B A_d(1 - \varepsilon_{Gd} - \varepsilon_{Sd})], \quad (19)$$

where the form friction loss coefficient (K_B) was calculated with equation (Chisti, 1989; Chisti et al., 1988):

$$K_B = 11.40 \left(\frac{A_d}{A_b} \right)^{0.79}, \quad (20)$$

where A_b is the area for flow under the baffle (Chisti et al., 1988). The K_B -value was 5.87.

Energy dissipation due to circulating fluid in wakes behind bubbles in the riser was estimated as recommended by Chisti et al. (1988):

$$E_R = E_{in} - \rho_L g h_D U_{Lr} A_r (\varepsilon_{Gr} + \varepsilon_{Sr}). \quad (21)$$

Similarly, the energy loss rate due to drag of gas on liquid in the downcomer was obtained as follows (Chisti et al., 1988)

$$E_D = \rho_L g h_D U_{Ld} A_d (\varepsilon_{Gd} + \varepsilon_{Sd}), \quad (22)$$

where the superficial liquid velocity in the downcomer was calculated from measured V_{Ld} (Ganzeveld et al., 1995):

$$U_{Ld} = V_{Ld}(1 - \varepsilon_{Gd} - \varepsilon_{Sd}). \quad (23)$$

Note that any energy dissipation in the head zone of the reactor was disregarded as being negligible relative to the other dissipation terms in split-cylinder and concentric draft tube types of internal-loop reactors that are relevant to animal cell culture (Chisti et al., 1988; Chisti, 1989).

3.2. Shear stress

The definition of shear stress previously employed (Merchuk and Ben-Zvi, 1992; Merchuk and Berzin, 1995) for bubble columns was modified for application to airlift reactors. Thus, knowledge of the energy dissipation rate and the fluid residence time in any zone of the reactor was used to calculate the shear rate in that zone:

$$\tau_i = \frac{E_i t_{ri}}{h_i V_i (a_i + a_{Si})}. \quad (24)$$

Here τ_i , E_i and t_{ri} are the values of shear stress, energy dissipation rate and residence time respectively in zone i (i =riser, downcomer and the bottom zone). The h_i and V_i in Eq. (24) are the height and the volume of zone i . Based on the information provided by Ganzeveld et al. (1995), h_i -values were identical for the riser and the downcomer in any given reactor; the values were either 0.315 m, or 0.70 m. The h_i -values for the head and the bottom zones were 0.06 and 0.05 m, respectively. The specific interfacial areas of bubbles (a_i) and microcarriers (a_{Si}) in any zone i were calculated from the gas and solids holdups in those zones:

$$a_i = \frac{6\varepsilon_{Gi}}{d_B} \quad (25)$$

and

$$a_{Si} = \frac{6\varepsilon_{Si}}{d_p} \quad (26)$$

The hydraulic residence times of liquid in the various zones were obtained with the following equations:

$$t_{tr} = \frac{h_r}{V_{Lr}} (1 - \varepsilon_{Gr} - \varepsilon_{Sr}) \quad (27)$$

for the riser;

$$t_{rd} = \frac{h_d}{V_{Ld}} (1 - \varepsilon_{Gd} - \varepsilon_{Sd}) \quad (28)$$

for the downcomer; and

$$t_{rb} = \frac{V_b}{V_{Ld}A_d} (1 - \varepsilon_{Gd} - \varepsilon_{Sd}). \quad (29)$$

In Eq. (29), V_b is the volume of the bottom zone ($= 8.9 \times 10^{-5} \text{ m}^3$).

3.3. Shear rate

The mean bulk shear rate in any region was calculated from the shear stress in that zone (Eq. (24)) and the viscosity of the solid-liquid slurry (Eq. (14)):

$$\gamma_i = \frac{\tau_i}{\mu_L} \quad (30)$$

For interpretation of shear rates around microcarriers, Kolmogoroff's isotropic turbulence model was used to calculate the length scale l_i of the energy dissipating microeddies; thus

$$l_i = \left(\frac{\mu_L^3}{\rho_L^3 E_{im}} \right)^{1/4} \quad (31)$$

In Eq. (31), E_{im} is the rate of energy dissipation per unit mass in zone i ; it is calculated as

$$E_{im} = \frac{E_i}{\rho_L V_i} \quad (32)$$

The turbulent shear rate around the microcarriers was calculated with the equation

$$\gamma_m = \psi \left(\frac{\rho_L}{\mu_L} \right)^2 E_{im} d_p^2 \quad (33)$$

Eq. (33) derives from the shear stress relationship of Matsuo and Unno (1981) as cited by Croughan et al. (1987). Because the hydrodynamic shear

Table 1
Geometric details of split-cylinder airlift reactors^a

Reactor	1	2
Overall height (m)	0.52	0.91
Column diameter (m)	0.056	0.056
Liquid height (m)	0.425	0.81
Working volume $\times 10^3$ (m ³)	0.93	1.75
Baffle		
Width (m)	0.055	0.055
Height (m)	0.315	0.70
Thickness (m)	0.001	0.001

^a Ganzeveld et al. (1995)

stress threshold for damage to anchored cells is about 1 N m^{-2} (Stathopoulos and Hellums, 1985; Ziegelstein et al., 1992), but the maximum shear stress value obtained from the original equation of Matsuo and Unno (1981) under conditions that damaged cells (Croughan et al., 1987) was about 0.5 N m^{-2} , we believe that a low value of ψ ($= 0.37$) was used in the original equation. Based on this reasoning, we used a ψ -value of 0.74 in Eq. (33).

4. Experimental details

Data presented by Ganzeveld et al. (1995) for two split-cylinder internal-loop airlift reactors were used in the analyses reported here. The reactors consisted of glass tubes partitioned into risers and downcomers by stainless steel baffles. In both cases, the riser-to-downcomer cross sectional area ratios were unity. The two reactors had different aspect ratios at 7.6 and 14.5. In both cases, the clearance of the baffles above the sparger was 0.05 m; the clearance between the top of the baffles and the static solid-liquid slurry was 0.06 m. All other dimensions are detailed in Table 1. The reactors were sparged through a sintered glass sparger ($1.5 \times 10^{-2} \text{ m}$ diameter; $110 \times 10^{-6} \text{ m}$ pore size) located at the base of the riser (Ganzeveld et al., 1995). The riser superficial air velocity range was $0\text{--}6.7 \times 10^{-3} \text{ m s}^{-1}$; the corresponding specific power inputs were $0\text{--}33 \text{ W m}^{-3}$ (Ganzeveld et al., 1995). Bubble diameters were estimated by visual inspection; the diameters

Table 2
Bubble diameters in microcarrier-free salt solution

$U_{Gr} \times 10^3$ (m s ⁻¹)	d_B (riser) (mm)	d_B (downcomer) (mm)
<1.6	0.5	0.3
1.6–3.9	1.0	0.7
>3.9	1.5	1.0

depended on aeration rate as shown in Table 2. Sodium chloride (0.1 kmol m⁻³) in deionized water was used to simulate the ionic strength of typical cell culture media (Ganzeveld et al., 1995). Three types of microcarriers were tested as detailed in Table 3. The Cole-Parmer microcarriers (Table 3) were sieved into two size fractions: (I) (160–212) × 10⁻⁶ m particle diameter; and (II) (212–300) × 10⁻⁶ m diameter for comparisons based on particle size differences (Ganzeveld et al., 1995). The solids loadings (based on liquid feed) in the reactors varied over 0–30 kg m⁻³, covering the typical range of loadings used in microcarrier culture. The procedures used for measurements of the overall gas holdup and the liquid velocity are detailed by Ganzeveld et al. (1995).

5. Results and discussion

The power inputs and dissipation rates in various zones of the two reactors are shown in Fig. 2 for a microcarrier-free two-phase system. Because the two reactors had identical diameters and A_r/A_d ratios, the specific power inputs in them were equal at identical gas velocities. However, as shown in Fig. 2, the absolute values of the power

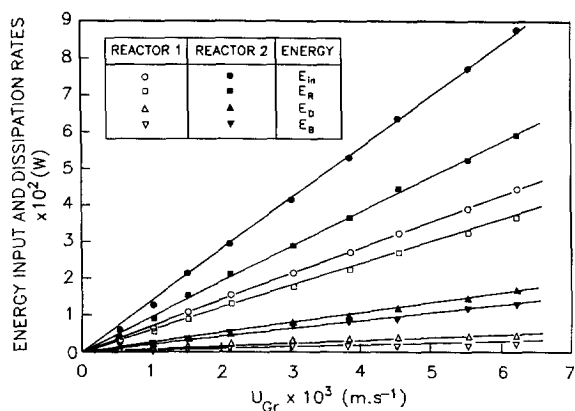


Fig. 2. Energy input (E_{in}) and dissipation rates in the riser (E_R), the downcomer (E_D) and the bottom (E_B) zones of reactors 1 and 2 for various values of riser superficial gas velocity. Effects of aspect ratio is shown in solids-free system.

input rate (E_{in}) were different in the two vessels because the aspect ratios and, hence, the liquid volumes were not the same. Reactor 2 had ~ 1.88-fold the volume of reactor 1; consequently, the absolute power input in reactor 2 was about two-fold that in reactor 1 (Fig. 2). For both vessels, the absolute rates of energy dissipation increased in the order: bottom region < downcomer < riser (Fig. 2). The dissipation rates increased linearly with the superficial gas velocity. In general, the energy input rate tended to be slightly higher than the sum of the dissipation rates E_R , E_D and E_B , because other minor energy dissipation terms such as the effects of the head region, bubble rupture at the surface and bubble formation at the sparger were not considered in the energy balance propounded by Chisti et al. (1988). That approach was justified as confirmed by the insubstantial differences between the input and the dissipation terms in Fig. 2.

Table 3
Properties of microcarriers^a

Manufacturer	Material	Density (kg m ⁻³)	Diameter × 10 ⁶ (m)
Sigma	Glass-coated plastic	1030	150–210
SoloHill	Glass-coated plastic	1040	150–210
Cole-Parmer	Polystyrene	1050	160–300

^a Ganzeveld et al. (1995)

While the absolute rates of energy dissipation as in Fig. 2 need to be known to characterize the contribution of various zones, the turbulence, the shear stress and the shear rate are determined not by the absolute amount of energy but by specific energy dissipation rates. Data on specific energy dissipation rates in various regions of reactor 2 are presented in Fig. 3. The figure reveals that the bottom zone experienced the highest specific dissipation rates (because of the small volume of that zone) even though the absolute rates of dissipation in the bottom were lower than elsewhere in the vessel (Fig. 2). The specific rate of energy dissipation was generally significantly higher in the riser than in the downcomer despite the virtually identical volumes of those two zones ($A_r/A_d = 1.0$). This result was consistent with the general visual observations of far less chaotic flow in downcomers of airlift vessels than in risers (Chisti, 1989). Some of the energy in the downcomer is lost to compressing the gas bubbles as they move down the downcomer (Chisti, 1989). This energy, as well as possibly higher rates of dissipation at the point of gas injection in the bottom zone contribute to turbulence in that zone. The specific energy dissipation rates in all zones increased with increasing gas flow rate (Fig. 3), but the rate of increase was significantly greater in the riser than in the downcomer. Over the greater range of gas flow velocities tested, the rates of increase in

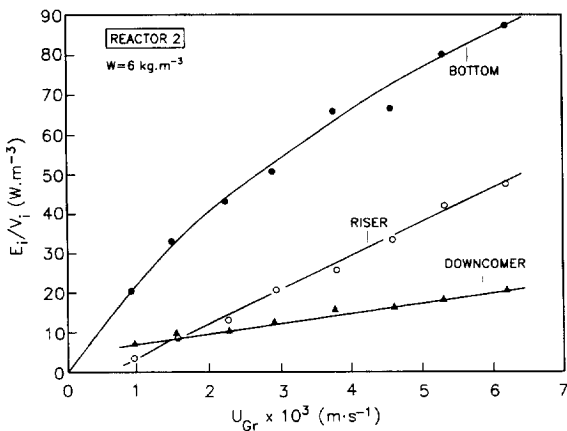


Fig. 3. Specific energy dissipation rate in riser, downcomer and bottom zones of reactor 2. Effect of aeration rate (SoloHill microcarriers).

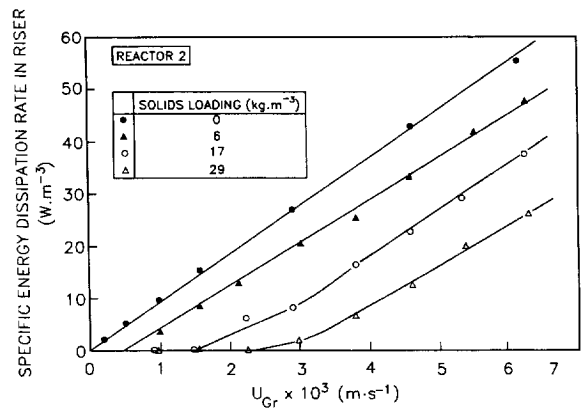


Fig. 4. Energy dissipation rate in the riser per unit riser volume in reactor 2. Effects of SoloHill microcarrier loading and aeration rate are shown.

specific energy dissipation in the riser and the bottom zones were comparable (Fig. 3). The data in Fig. 3 were typical of all solids loadings in the two reactors.

The specific energy dissipation rates in all zones decreased with increasing solids loading. This is illustrated in Fig. 4 for the riser. Increasing concentration of solids is known to lower the induced liquid circulation velocity (Ganzeveld et al., 1995), mainly by lowering the riser gas holdup, but also because of the increased viscosity of the slurry.

Changes in particle density and diameter within the small ranges that are relevant to microcarrier culture have only slight effects on shear rate as shown in Fig. 5 and Fig. 6. Larger or denser

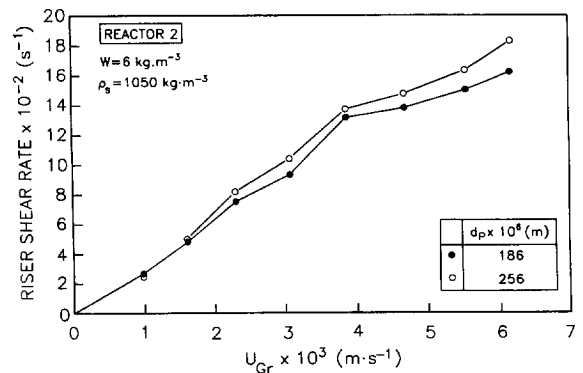


Fig. 5. Effects of microcarrier size and the riser superficial gas velocity on shear rate in riser (Cole-Parmer microcarriers).

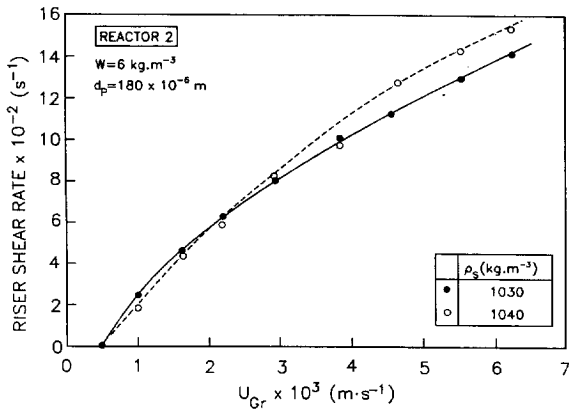


Fig. 6. Effects of microcarrier density and the riser superficial gas velocity on shear rate in riser.

microcarriers experience greater shear rates. These effects result mainly from the impact of particle size and density on gas holdup.

The effect of aeration rate and solids loading on the overall or global shear rate is shown in Fig. 7. In general, the shear rates are much higher in solids-free systems, but not particularly sensitive to solids loading beyond 6 kg m⁻³. The global shear rate is significantly affected by the diameter of microcarrier as shown in Fig. 8. This is because the higher shear rates in the bottom zone are more sensitive to variations in properties of microcarriers than the lower shear rates in the riser. Thus, a non-linear dependence of shear rate on properties of carriers is revealed. The global

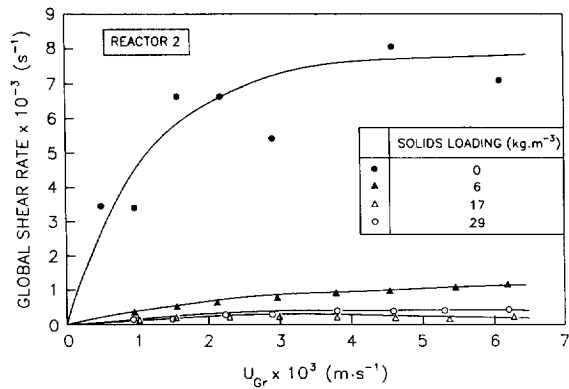


Fig. 7. Global shear rate versus riser superficial gas velocity. Effect of solids loading (SoloHill microcarriers).

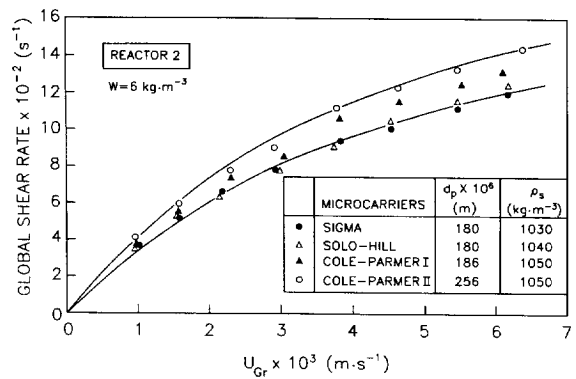


Fig. 8. Effects of microcarrier type (density and diameter) and aeration rate on global shear rate in reactor 2.

shear rates in Fig. 7 and Fig. 8 were calculated from the mean shear rates in the riser, the down-comer and the bottom zones; thus,

$$\gamma = \frac{\sum V_i \dot{\gamma}_i}{\sum V_i} \tag{34}$$

The shear rates in various zones of reactor 2 as functions of the specific energy dissipation rates in the relevant zones are depicted in Fig. 9 for the system with 6 kg m⁻³ microcarrier loading. Again, for any level of specific energy dissipation, the shear rates in the bottom zone are the highest.

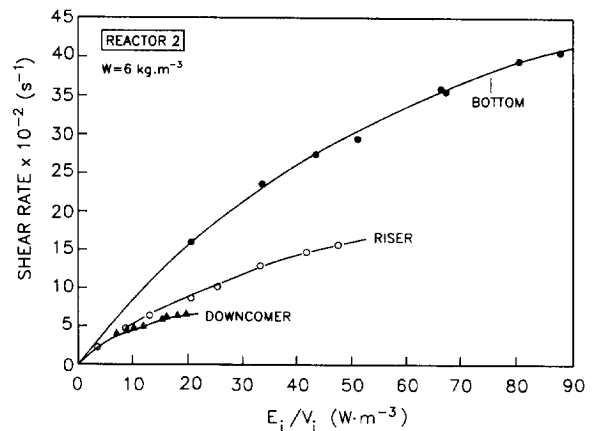


Fig. 9. Shear rate variations in riser, downcomer and bottom zones of reactor 2 as a function of specific energy dissipation rates in those zones (SoloHill microcarriers).

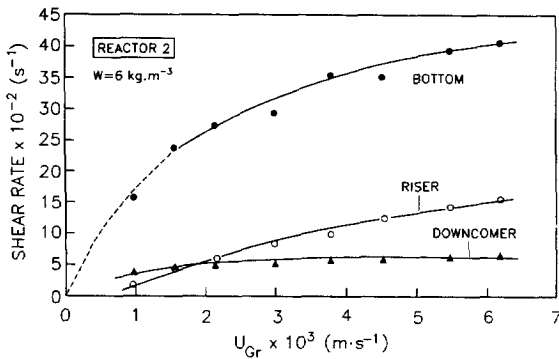


Fig. 10. Shear rate variations in riser, downcomer and bottom zones of reactor 2 as a function of riser gas flow rate (SoloHill microcarriers).

The shear rate values in the other two zones are fairly similar, but the downcomer is consistently the most quiescent (Fig. 9). The higher shear rates in the bottom zone are associated with the turnaround flow through a restricted area under the baffle. For practical purposes, the effect of the aeration rate on shear rate is also of interest. Typically, the shear rate increased in every zone with increasing aeration rate in the riser (Fig. 10); however, the downcomer zone was the least sensitive to this effect.

Note that the forms of the shear rate-aeration rate curves in Fig. 7, Fig. 8 and Fig. 10 are consistent with the behaviour shown in Fig. 1 for shear rate derived from the fundamental Eq. (3). The several empirical linear relationships of the type $\gamma = \delta \cdot U_G$ that have been proposed for bubble columns (see Chisti and Moo-Young, 1989; Chisti, 1989) with δ -values in the range 1500–5000 m⁻¹ are not consistent with the behaviour observed in this work, with the fundamental Eq. (3), or with the empirical relationship of Shi et al. (1990).

Of further note is the fact that the shear rate values calculated using Eq. (2) and Eq. (3) (Fig. 1) are extremely low relative to those seen in Fig. 10. This disparity is explained by the fact that shear rate in the laminar sublayer at the wall is low in comparison with shear rates in the turbulent core in a flow channel. Both Eq. (2) and Eq. (3) are measures of wall shear rate. In contrast, the shear rate data in Fig. 10 (and elsewhere in this work)

are for the bulk flow in various zones, conditions in bulk flow being of greater relevance to shear-sensitive processes than are the wall shear rate data.

From Fig. 10, the shear rates in airlift bioreactors can be seen to range over 250–4000 s⁻¹ for the operational conditions that are typical of animal cell culture. These shear rates are substantially lower than the value of $\sim 10^5$ s⁻¹ that would be required to damage cells if the 100 N m⁻² shear stress value (Born et al., 1992; Doran, 1993) is taken to be the threshold of mechanical damage. However, based on the shear stress data of Olivier and Truskey (1993), during the process of attachment of cells to microcarriers, shear rate levels of 250–600 s⁻¹ may well be detrimental. Thus, during initial attachment of cells, the reactor would need to be operated at reduced aeration rates—a practice that is well established through empirical experience, but previously explained only intuitively.

The shear rate in the riser declines as the characteristic length of the turbulent eddies (Eq. (31)) in the fluid increases (Fig. 11). The greatest change in shear rate occurs over a narrow range of eddy sizes. For a fixed eddy length, the riser shear rate declines with increasing loading of solids (Fig. 11). For hydrodynamic damage to cells anchored on microcarriers, mechanistic reasoning suggests that the length scale of eddies should be less than or equal to the dimensions of the carriers. Thus, the riser shear rate is plotted in Fig. 12 as a function of the eddy length-to-micro-

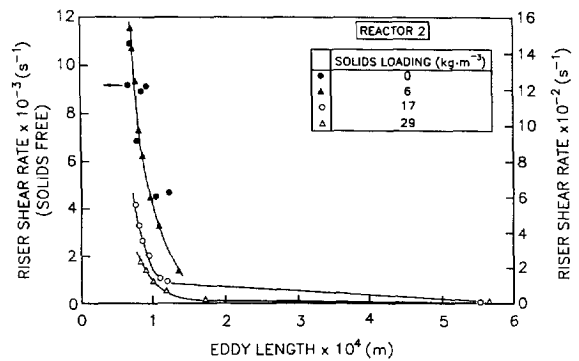


Fig. 11. Riser shear rate as a function of Kolmogoroff eddy length and solids loading (SoloHill microcarriers).

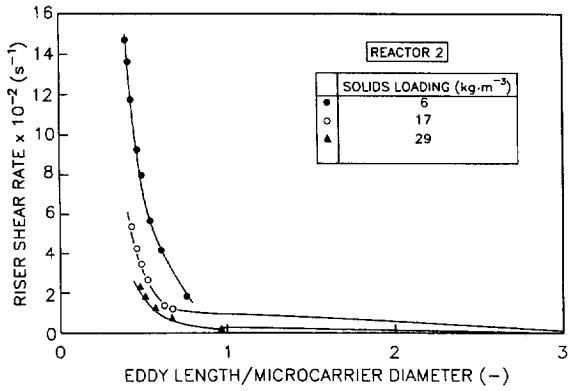


Fig. 12. Riser shear rate as a function of eddy-to-microcarrier size ratio for various loadings of SoloHill microcarriers.

carrier diameter ratio, l_i/d_p . Note that the cells would experience a rapid increase in shear rate as the l_i/d_p ratio declines to ≤ 1 (Fig. 12 and Fig. 13). As seen in Fig. 13, the shear rate is highest in the bottom zone for any value of the l_i/d_p ratio. The shear characteristics of the bottom zone may be advantageously modified by altering the geometry of the zone so that the velocity of flow is reduced and the volume of the zone is enlarged. Similarly, inspection of Eq. (19), Eq. (20) and Eq. (21) suggests ways of modifying the hydrodynamic shear environment of other zones.

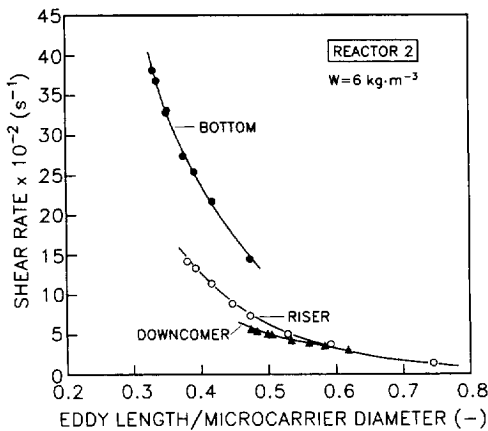


Fig. 13. Shear rate variations in riser, downcomer and bottom zones of reactor 2 as functions of eddy-to-microcarrier size ratio (SoloHill microcarriers).

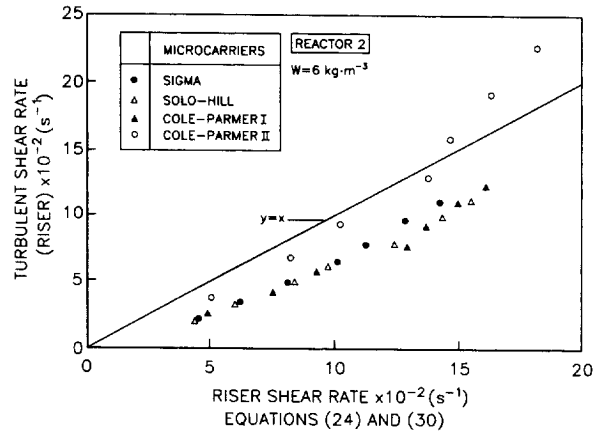


Fig. 14. Comparison of turbulent shear rate (Eq. (33)) in riser with values derived from Eq. (24) and Eq. (30) for various types of microcarriers.

The shear rates in the riser calculated with Eq. (33) and with the model developed in this work are compared in Fig. 14 for several types of microcarriers. A similar comparison is shown in Fig. 15 for shear rates in the riser, the downcomer and the bottom zones. For most of the data, Eq. (33) underpredicts the shear rate (Fig. 14 and Fig. 15), but generally the two models agree well within $\pm 50\%$.

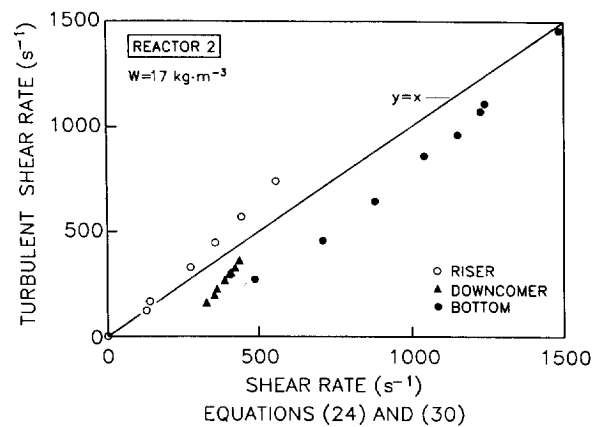


Fig. 15. Comparison of turbulent shear rate (Eq. (33)) with values calculated using Eq. (24) and Eq. (30) for the riser, the downcomer and the bottom zones (SoloHill microcarriers).

6. Conclusions

An energy dissipation approach was used to characterize the bulk flow shear rates in the riser, the downcomer and the bottom zones of split-cylinder airlift bioreactors for animal cell culture. For any aeration rate, the specific energy dissipation rates increased in the order: downcomer < riser < bottom. The dissipation rates in any zone declined with increasing loading of microcarriers. The behaviour of shear rates in any zone corresponded to that of the specific energy dissipation rate. The shear rates were not particularly sensitive to the density or the diameter of microcarriers within the ranges that are relevant to anchorage dependent cell culture. Typical shear rates ranged over 250–4000 s⁻¹ in the microcarrier containing systems, but much higher values, up to 12 000 s⁻¹, were noted for solids-free media. These values compared favourably with shear rates of ~ 10⁵ s⁻¹ that have been reported to be the threshold of damage to cells. The data showed that the cells would experience a substantial increase in the riser shear rate only when the fluid eddy length-to-microcarrier diameter ratio declined to ≤ 1. The shear rates calculated from the energy dissipation model agreed satisfactorily with those obtained from the model proposed by Matsuo and Unno (1981). The methodology developed here for characterization of shear rates in specific zones, as opposed to undifferentiated 'global' shear rates or wall shear rates, provides a better understanding of how the operational and geometric factors may be manipulated to attain less detrimental levels of shear in airlift bioreactors.

7. Nomenclature

A_b	cross-sectional area for flow under the baffle (m ²)
-------	------------------------------------------------------------------

A_d	cross-sectional area of the downcomer (m ²)
A_r	cross-sectional area of the riser (m ²)
a_i	specific gas-liquid interfacial area in zone i (m ⁻¹)

a_{Si}	specific solid-liquid interfacial area in zone i (m ⁻¹)
C_f	friction factor (–)
d_B	bubble diameter (m)
d_c	diameter of bubble column (m)
d_p	microcarrier diameter (m)
d_r	hydraulic diameter of riser (m)
E_B	energy dissipation rate for fluid turnaround at the bottom (W)
E_D	energy dissipation due to stagnant bubbles in downcomer (W)
E_F	energy dissipation rate due to wall friction (W)
E_i	energy dissipation rate in zone i (W)
E_{im}	energy dissipation rate per unit mass in zone i (W kg ⁻¹)
E_{in}	energy input rate (W)
E_R	energy dissipation rate due to wakes behind bubbles in riser (W)
g	gravitational acceleration (m s ⁻²)
h_D	height of gas-liquid dispersion (m)
h_d	height of downcomer (m)
h_i	height of zone i (m)
h_L	height of gas-free liquid (m)
h_r	height of riser (m)
K_B	friction loss coefficient for fluid turnaround at bottom (–)
k_d	death rate constant (s ⁻¹)
l_i	length of energy dissipating microeddies in zone i (m)
P_a	absolute atmospheric pressure (Pa)
Q	volume flow rate of gas (m ³ s ⁻¹)
t_{rb}	liquid residence time in the bottom zone (s)
t_{rd}	liquid residence time in downcomer (s)
t_{ri}	liquid residence time in zone i (s)
t_{rr}	liquid residence time in riser (s)
U_G	superficial velocity of gas in bubble column (m s ⁻¹)
U_{Gr}	superficial velocity of gas in riser (m s ⁻¹)
U_{Ld}	superficial velocity of liquid in downcomer (m s ⁻¹)
U_{Lr}	superficial velocity of liquid in riser (m s ⁻¹)
V_b	volume of the bottom zone (m ³)
V_i	volume of zone i (m ³)
V_k	dimensionless hypothetical specific killing volume (–)

V_{Ld} linear velocity of liquid in downcomer (m s⁻¹)
 V_{Lr} linear velocity of liquid in riser (m s⁻¹)
 W solids loading (kg m⁻³)

Greek symbols

δ empirical constant (m⁻¹)
 ε_G overall gas holdup (—)
 ε_{Gd} volume fraction of gas in the downcomer (—)
 ε_{Gi} volume fraction of gas in zone i (—)
 ε_{Gr} volume fraction of gas in the riser (—)
 ε_{Gb} volume fraction of gas in the bottom zone (—)
 ε_{Sd} volume fraction of solids in the downcomer (—)
 ε_{Si} volume fraction of solids in zone i (—)
 ε_{Sr} volume fraction of solids in the riser (—)
 ε_{Sb} volume fraction of solids in the bottom zone (—)
 ϕ_S volume fraction of solids based on loading in gas-free two-phase slurry (—)
 ρ_L density of liquid or slurry (kg m⁻³)
 ρ_S density of microcarriers (kg m⁻³)
 τ_i shear stress in zone i (N m⁻²)
 τ_w wall shear stress (N m⁻²)
 γ average overall shear rate (s⁻¹)
 γ_i shear rate in zone i (s⁻¹)
 γ_m shear rate (Eq. (33)) around microcarriers (s⁻¹)
 γ_w wall shear rate (s⁻¹)
 μ_L viscosity of slurry (Pa·s)
 μ_{Lw} viscosity of liquid (Pa·s)
 ψ constant in Eq. (33) (—)
 π Pi (—)

References

- Al-Rubeai, M., Emery, A.N., Chalder, S. and Goldman, M.H. (1993) A flow cytometric study of hydrodynamic damage to mammalian cells. *J. Biotechnol.* 31, 161–177.
- Arathoon, W.R. and Birch, J.R. (1986) Large-scale cell culture in biotechnology. *Science* 232, 1390–1395.
- Bavarian, F., Fan, L.S. and Chalmers, J.J. (1991) Microscopic visualization of insect cell-bubble interactions. I: Rising bubbles, air-medium interface, and the foam layer. *Biotechnol. Prog.* 7, 140–150.
- Bello, R.A. (1981) A characterization study of airlift contactors for applications to fermentations. PhD thesis, University of Waterloo, Canada.
- Birch, J.R., Lambert, K., Thompson, P.W., Kenney, A.C. and Wood, L.A. (1987) Antibody production with airlift fermentors. In: Lydersen, B.K. (Eds.), *Large Scale Cell Culture Technology*, Hanser, New York, pp. 1–20.
- Born, C., Zhang, Z., Al-Rubeai, M. and Thomas, C.R. (1992) Estimation of disruption of animal cells by laminar shear stress. *Biotechnol. Bioeng.* 40, 1004–1010.
- Boulton-Stone, J.M. and Blake, J.R. (1993) Gas bubbles bursting at a free surface. *J. Fluid Mech.* 254, 437–466.
- Chalmers, J.J. and Bavarian, F. (1991) Microscopic visualization of insect cell-bubble interactions. II: The bubble film and bubble rupture. *Biotechnol. Prog.* 7, 151–158.
- Chattopadhyay, D., Rathman, J.F. and Chalmers, J.J. (1995a) The protective effect of specific medium additives with respect to bubble rupture. *Biotechnol. Bioeng.* 45, 473–480.
- Chattopadhyay, D., Rathman, J.F. and Chalmers, J.J. (1995b) Thermodynamic approach to explain cell adhesion to air-medium interfaces. *Biotechnol. Bioeng.* 48, 649–658.
- Cherry, R.S. and Papoutsakis, E.T. (1986) Hydrodynamic effects on cells in agitated tissue culture reactors. *Bioprocess Eng.* 1, 29–41.
- Cherry, R.S. and Papoutsakis, E.T. (1988) Physical mechanisms of cell damage in microcarrier cell culture bioreactors. *Biotechnol. Bioeng.* 32, 1001–1014.
- Cherry, R.S. and Papoutsakis, E.T. (1989) Growth and death rates of bovine embryonic kidney cells in turbulent microcarrier bioreactors. *Bioprocess Eng.* 4, 81–89.
- Chisti, Y. (1989) *Airlift Bioreactors*, Elsevier, London.
- Chisti, Y. (1993) Animal cell culture in stirred bioreactors: Observations on scale-up. *Bioprocess Eng.* 9, 191–196.
- Chisti, Y. and Moo-Young, M. (1986) Disruption of microbial cells for intracellular products. *Enzyme Microb. Technol.* 8, 194–204.
- Chisti, Y. and Moo-Young, M. (1989) On the calculation of shear rate and apparent viscosity in airlift and bubble column bioreactors. *Biotechnol. Bioeng.* 34, 1391–1392.
- Chisti, Y. and Moo-Young, M. (1996) Bioprocess intensification through bioreactor engineering. *Trans. Inst. Chem. Eng.* 74A, 575–583.
- Chisti, Y., Halard, B. and Moo-Young, M. (1988) Liquid circulation in airlift reactors. *Chem. Eng. Sci.* 43, 451–457.
- Croughan, M.S., Hamel, J.-F. and Wang, D.I.C. (1987) Hydrodynamic effects on animal cells grown in microcarrier cultures. *Biotechnol. Bioeng.* 29, 130–141.
- Doran, P.M. (1993) Design of reactors for plant cells and organs. *Adv. Biochem. Eng. Biotechnol.* 48, 115–168.
- Ganzeveld, K.J., Chisti, Y. and Moo-Young, M. (1995) Hydrodynamic behaviour of animal cell microcarrier suspensions in split-cylinder airlift bioreactors. *Bioprocess Eng.* 12, 239–247.
- Garcia-Briones, M.A. and Chalmers, J.J. (1992) Cell-bubble interactions: Mechanisms of suspended cell damage. *Ann. N.Y. Acad. Sci.* 665, 219–229.

- García-Briones, M.A. and Chalmers, J.J. (1994) Flow parameters associated with hydrodynamic cell injury. *Biotechnol. Bioeng.* 44, 1089–1098.
- García-Briones, M.A., Brodkey, R.S. and Chalmers, J.J. (1994) Computer simulations of the rupture of a gas bubble at a gas-liquid interface and its implications in animal cell damage. *Chem. Eng. Sci.* 49, 2301–2320.
- Handa, A., Emery, A.N. and Spier, R.E. (1987) On the evaluation of gas-liquid interfacial effects on hybridoma viability in bubble column bioreactors. *Dev. Biol. Stand.* 66, 241–253.
- Handa-Corrigan, A., Emery, A.N. and Spier, R.E. (1989) Effect of gas-liquid interfaces on the growth of suspended mammalian cells: mechanisms of cell damage by bubbles. *Enzyme Microb. Technol.* 11, 230–235.
- Jan, D.C.H., Emery, A.N. and Al-Rubeai, M. (1993) Use of a spin-filter can reduce disruption of hybridoma cells in a bioreactor. *Biotechnol. Techniques* 7, 351–356.
- Martens, D.E., de Gooijer, C.D., Beuvery, E.C. and Tramper, J. (1992) Effect of serum concentration on hybridoma viable cell density and production of monoclonal antibodies in CSTRs and on shear sensitivity in air-lift loop reactors. *Biotechnol. Bioeng.* 39, 891–897.
- Matsuo, T. and Unno, H. (1981) Forces acting on floc and strength of floc. *J. Env. Eng. Div. Am. Soc. Civ. Eng.* 107, 527–545.
- Merchuk, J.C. and Ben-Zvi (Yona), S. (1992) A novel approach to the correlation of mass transfer rates in bubble columns with non-newtonian liquids. *Chem. Eng. Sci.* 47, 3517–3523.
- Merchuk, J.C. and Berzin, I. (1995) Distribution of energy in airlift reactors. *Chem. Eng. Sci.* 50, 2225–2233.
- Michaels, J.D. and Papoutsakis, E.T. (1991) Polyvinyl alcohol and polyethylene glycol as protectants against fluid-mechanical injury of freely-suspended animal cells (CRL 8018). *J. Biotechnol.* 19, 241–258.
- Michaels, J.D., Kunas, K.T. and Papoutsakis, E.T. (1992) Fluid-mechanical damage of freely-suspended animal cells in agitated bioreactors: Effects of dextran, derivatized celluloses and polyvinyl alcohol. *Chem. Eng. Commun.* 118, 341–360.
- Michaels, J.D., Nowak, J.E., Mallik, A.K., Koczo, K., Wasan, D.T. and Papoutsakis, E.T. (1995a) Analysis of cell-to-bubble attachment in sparged bioreactors in the presence of cell-protecting additives. *Biotechnol. Bioeng.* 47, 407–419.
- Michaels, J.D., Nowak, J.E., Mallik, A.K., Koczo, K., Wasan, D.T. and Papoutsakis, E.T. (1995b) Interfacial properties of cell culture media with cell-protecting additives. *Biotechnol. Bioeng.* 47, 420–430.
- Olivier, L.A. and Truskey, G.A. (1993) A numerical analysis of forces exerted by laminar flow on spreading cells in a parallel plate flow chamber assay. *Biotechnol. Bioeng.* 42, 963–973.
- Papoutsakis, E.T. (1991) Fluid-mechanical damage of animal cells in bioreactors. *Trends Biotechnol.* 9, 427–437.
- Ramírez, O.T. and Mutharasan, R. (1990) The role of the plasma membrane fluidity on the shear sensitivity of hybridomas grown under hydrodynamic stress. *Biotechnol. Bioeng.* 36, 911–920.
- Ramírez, O.T. and Mutharasan, R. (1992) Effect of serum on the plasma membrane fluidity of hybridomas: An insight into its shear protective mechanism. *Biotechnol. Prog.* 8, 40–50.
- Shi, L.K., Riba, J.P. and Angelino, H. (1990) Estimation of effective shear rate for aerated non-Newtonian liquids in airlift bioreactor. *Chem. Eng. Commun.* 89, 25–35.
- Smith, C.G. and Greenfield, P.F. (1992) Mechanical agitation of hybridoma suspension cultures: Metabolic effects of serum, Pluronic F68, and albumin supplements. *Biotechnol. Bioeng.* 40, 1045–1055.
- Stathopoulos, N.A. and Hellums, J.D. (1985) Shear stress effects on human embryonic kidney cells in vitro. *Biotechnol. Bioeng.* 27, 1021–1026.
- Tramper, J., Smit, D., Straatman, J. and Vlák, J.M. (1987) Bubble column design for growth of fragile insect cells. *Bioprocess Eng.* 2, 37–41.
- Trinh, K., García-Briones, M., Hink, F. and Chalmers, J.J. (1994) Quantification of damage to suspended insect cells as a result of bubble rupture. *Biotechnol. Bioeng.* 43, 37–45.
- van der Pol, L., Bakker, W.A.M. and Tramper, J. (1992) Effect of low serum concentrations (0–2.5%) on growth, production, and shear sensitivity of hybridoma cells. *Biotechnol. Bioeng.* 40, 179–182.
- Wang, N.S., Yang, J.-D., Calabrese, R.V. and Chang, K.-C. (1994) Unified modelling framework of cell death due to bubbles in agitated and sparged bioreactors. *J. Biotechnol.* 33, 107–122.
- Zhang, Z., Chisti, Y. and Moo-Young, M. (1995) Effects of the hydrodynamic environment and shear protectants on survival of erythrocytes in suspension. *J. Biotechnol.* 43, 33–40.
- Ziegelstein, R.C., Cheng, L., Capogrossi, M.C. (1992) Flow-dependent cytosolic acidification of vascular endothelial cells. *Science* 258, 656–659.